View Article Online
View Journal

Dalton Transactions

An international journal of inorganic chemistry

Accepted Manuscript

This article can be cited before page numbers have been issued, to do this please use: T. Keyes, K. S. Gkika and A. Byrne, *Dalton Trans.*, 2019, DOI: 10.1039/C9DT02967B.

ROYAL SOCIETY OF CHEMISTRY

rsc.li/dalton

ROYAL SOCIETY OF CHEMISTRY View Article Online
DOI: 10.1039/C9DT02967B

Dalton Transactions

PAPER

Mitochondrial Targeted Osmium Polypyridyl Probe Shows Concentration dependent Uptake, Localisation and Mechanism of Cell Death.

Karmel Sofia Gkika, Aisling Byrne and Tia E. Keyes*

Received 00th January 20xx,
Accepted 00th January 20xx

DOI: 10.1039/x0xx00000x
www.rsc.org/

A symmetric Osmium(II) [bis- (4'-(4-carboxyphenyl)-2,2' :6', 2"- terpyridine)] was prepared and conjugated to two mitochondrial-targeting peptide sequences; FrFKFrFK (r= D-arginine). The parent and conjugate complexes showed strong near infra-red emission centred at λ_{max} 745nm that was modestly oxygen dependent in the case of the parent and oxygen independent in the case of the conjugate, attributed in the latter case, surprisingly, to a shorter emission lifetime of the conjugate compared to the parent. Confocal fluorescence imaging of sub-live HeLa and MCF 7 cells showed the parent complex was cell impermeable whereas the conjugate was rapidly internalised into the cell and distributed in a concentration dependent manner. At concentrations below approximately 30 µmol, the conjugate localised to the mitochondria of both cell types where it was observed to trigger apoptosis induced by the collapse of the mitochondrial membrane potential (MPP). At concentrations exceeding 30 µmol the conjugate was similarly internalised rapidly but distributed throughout the cell, including to the nucleus and nucleolus. At these concentrations, it was observed to precipitate a caspase- dependent apoptotic pathway. The combination of concentration dependent organelle targeting, NIR emission coincident with the biological window, and distribution dependent cytotoxicity offers an interesting approach to theranostics with the possibility of eliciting site dependent therapeutic effect whilst monitoring the therapeutic effect with luminescence imaging.

Introduction

Mitochondria are the centres of cellular metabolism and like the nucleus are repositories for DNA in eukaryotic cells. Mitochondrial dysfunction, which often arises from mutation to mitochondrial DNA, is associated with numerous disease states including inflammatory diseases and cancer.[1,2] Consequently, molecular targeting to the mitochondrial has attracted significant attention, both in the fields of imaging/sensing and in the field of medicinal chemistry/therapeutics.[3,4] Cancer cells differ from normal cells in terms of their energy metabolism, ATP production, reactive oxygen species levels and present many dysfunctions. Therefore, targeted agents may be driven to interact with species that are upregulated in cancer cell mitochondria to achieve preferential targeting of cancer cells or accumulate within the organelle matrix environment depending on compound design and overall charge. A key role of mitochondria is ATP production driven by a membrane-based proton pump which generates an electrochemical gradient. This transmembrane electrical potential gradient, known as $\Delta\Psi_m$, is between -80 and -180 mV. Depolarization of the inner membrane of the mitochondrion typically results in loss of $\Delta\Psi_m$, due to release of proteins triggering apoptosis. Small molecules such as silver (I) complexes, pancratistatin alkaloid or rhodamine 123 are known to penetrate the mitochondria where they induce apoptosis via depolarization of the mitochondrial membrane potential (MMP).[5] Metallo-anticancer therapeutic agents have attracted interest since the breakthrough with cisplatin and DNA interaction in 1978.[6,7] Although cisplatin is used in cancer treatment, it is inevitably limited by resistance phenomena and several side effects such as nephron- and neuro-toxicity owing to the mode of action of the drug.[8] Ruthenium (III) compounds of

[a] School of Chemical Sciences, National Centre for Sensor Research, Dublin City University, Glasnevin, Dublin 9, Ireland. E-mail: tia.keyes@dcu.ie
†Electronic Supplementary Information (ESI) available: Spectra of parent complexes, lifetime decays, oxygen studies, ^{1}H NMR analysis, HPLC analysis
See DOI: 10.1039/x0xx00000x

similar structure to cisplatin have been investigated for their anticancer activity including some that have been clinically developed: KP1019[9], NKP1339 (IT- 139)[10,11] and NAMI-A[12,13]. Although more inert toward ligand substitution, osmium-based compounds have been shown to induce cell death via several pathways including inhibitory activity against kinases [14,15], endoplasmic reticulum stress and DNA damage[16–18] and redox dependent activation in targeted mitochondria of ovarian cancer cells.[19] Work by Sadler, Dyson and Keppler and their respective groups have revealed the potent antiproliferative activity of organometallic osmium complexes.[7,19,20] More recently,[21] the capability of osmium polypyridyl complexes in imaging and in phototherapy has started to be explored.[22–26] These studies emphasize that along with Ru- complexes, osmium structures can also offer additional coordination chemistry and rich redox and photochemistry leading to alternative pathways for inducing antiproliferative effects.[27,28] We have focused on the development of peptide conjugated metal complexes capable of organelle selective targeting.[29–31] The importance of efficient localization for multimodal use of transition-metal complexes has been highlighted by MD Ward in a recent publication concerning mitochondria-targeted Ir(III) complexes.[32] Luminescent mitochondrial or nuclear- targeting metal complexes can act as real-time imaging/sensing probes and as therapeutic/theranostic agents.[33–35] Although emission quantum yields are frequently lower, osmium polypyridyl complexes share many photophysical advantages with their ruthenium (II) analogues with the additional benefits of NIR emission maxima in spectral region coincident with the biological optical window and they exhibit outstanding photostability. Consequently they may be good alternatives to their ruthenium analogues as imaging probes because of their photostability.[36] To date there have been no examples of terpyridine-based ruthenium or osmium complexes applied in the context of cell imaging or therapy although such complexes have structural advantages compared to tris(bidentate) ligand bound complexes as they do not form stereoisomers. While stereoisomerism tends not to affect photophysical properties they can, in the biological context, affect recognition, which in turn can affect cytotoxicity as exemplified recently by Keene et al.[37] Furthermore, terpy ligands offer stepwise coordination permitting spatial separation of functionality at the 4 positions. In contrast to other polypyridyl ligands, terpyridine-based osmium complexes tend to be more luminescent than their ruthenium analogues. For example, whereas prototype $[Ru(terpy)_2]^{2+}$ barely emits at room temperature $[Os(terpy)_2]^{2+}$ emits relatively strong.[38] This has been attributed to relatively weak ligand field strength of tpy, that facilitates population of ^{3}MC states from the MLCT states at room temperature. This leads to rapid nonradiative decay and relatively poor photostability, which in the context of the cellular environment, will be exacerbated at temperatures typically used for cell culture. Hanan, Campagna and co-workers, have each reported clever strategies for improving the photophysical properties of Ru(II) terpy complexes through extension and rigidification of the terpy ligand.[39–41] Nonetheless, in contrast to biscoordinated ligand systems, osmium terpyridine complexes offer significant advantages over their ruthenium analogues in terms of quantum yield, photostability and emission wavelength.[42] We previously reported that in Ruthenium and Os(II) tris-ligand systems coordinated to polyarginines, Os(II) showed superior uptake/permeability, and notably lower cytotoxicity than their ruthenium analogues. We were interested to explore the performance of Os(II)terpy complexes in this regard to understand if they can be driven to organelles using peptides exploited in ruthenium complexes and also to exploit the symmetric nature of the terpy-like ligands to conjugate two peptides to a single complex.

Herein, we report on the preparation of a symmetric Osmium (II)- terpyridine conjugated to two mitochondrial targeting peptides $[Os(tpybenz\text{-}Ahx\text{-}MPP)_2]^{8+.}$ We examined its photophysical behavior, uptake and toxicity in live cells and compared behavior to its parent. The conjugate shows precision targeting to the mitochondria was relatively cytotoxic. The effect of the Os^{II} MPP probe on the mitochondrial membrane potential was studied in HeLa and MCF 7 cells and was found to be cytotoxic. Interestingly, however, the mechanism of cytotoxicity changed with concentration as distribution of the probe changed. This to our knowledge is the first metal complex baring two mitochondrial penetrating peptides (MPP) to be studied in cells and first MPP-driven Os (II) complex.

Materials and Methods

Materials

All chemicals and reagents, cell culture media and corresponding components were purchased from Sigma Aldrich (Ireland) and were used as received. The MPP peptide sequence was purchased from Celtek Peptides, Franklin, USA.

View Article Online
DOI: 10.1039/C9DT02967B

Co-localising dyes were purchased from Life Sciences and Resazurin agent from PromoKine.

Instrumentation

^{1}H and ^{13}C NMR spectra were recorded on a 400MHz Bruker Spectrophotometer and processed and calibrated against solvent peaks using Bruker Topspin (v2.1) software. High Resolution LCMS with ESI was performed at the Mass Spectrometry Facility, NUI Maynooth. Thin layer chromatography (TLC) was performed on glass silica gel (Merck, 250µm thickness) or C18 plates (Sorbent Technologies, 250µm thickness). Analytical HPLC was performed on a Varian 940-LC with a Photometric Diode Array (PDA) detector for peak detection monitoring 280 nm and 490 nm channels. Gradient elution was applied, using 0.1% v/v TFA in MeCN and deionised water using HICHROM C18 column (4.6 x 250mm). The mobile phase was of HPLC grade quality, filtered and purged with nitrogen prior to use. Prior to sample injection, samples were filtered (0.8µm pore size). Typical chromatographic run-times were 15-20 minutes at a flowrate of 1ml/min.

Electronic absorption spectra were acquired on a Jasco V670 UV/vis NIR spectrophotometer using a quartz cuvette with a pathlength of 1 cm. Fluorescence spectra were collected on a Varian Cary Eclipse Fluorescence Spectrofluorometer with background correction. All photophysical measurements were performed at room temperature (293 K). Luminescent lifetime data were acquired up to 10,000 counts using a Time Correlated Single Photon Counting (TCSPC) system by PicoQuant with laser excitation source a 450 nm. Measurements were performed in triplicate and PicoQuant NanoHarp software was used for data analysis and fitting.

Preparation of 4'- (4-Carboxyphenyl)-2,2' :6', 2''- terpyridine , (tpybenzCOOH)

4-formylbenzoic acid (179 mg, 1.2 mmol) was dissolved in stirring CH_3OH (8ml) followed by the addition of 2-Acetylpyridine (289 mg, 2.4 mmol). The mixture was allowed to stir for 5 minutes followed by the slow addition of 15% potassium hydroxide (7.2ml) and conc. ammonium hydroxide (0.8ml) resulting in a bright green solution which turned yellow over time. The mixture was allowed to stand at room temperature for 3 days. The yellow/white emulsion that formed was filtered off and washed with cold chloroform (2x2ml) and cold methanol/water (1:1) to yield a white product which was suspended in methanol/water (80:20) and sonicated at 35 °C until a yellow solution was obtained. The solution was transferred to a large beaker and acidified to pH 2 by addition of 1M hydrochloric acid while stirring for 10 minutes. The resulting white precipitate was collected by vacuum filtration, rinsed with ice water and allowed to dry overnight yielding pure white solids of tpybenzCOOH (297mg, 73%)

^{1}H NMR (400MHz, TFA-d): δ (ppm) 9.20 (dd, 2H, J= 5.2Hz), 8.98 (d, 2H, J= 0.8Hz), 8.90- 8.85 (s, dd, 4H, J*), 8.42 (dd, 2H, J= 1.2Hz, 9.2Hz), 8.28 (dd, 2H, J = 6.4Hz), 8.04 (dd, 2H, J = 1.2, 9.6Hz). ^{13}C NMR (600MHz, TFA-d): 154.44, 148.33, 147.49, 146.65, 142.49, 140.64, 131.46, 130.63, 128.21, 127.36.

Preparation of $[Os(4'-(4-Carboxyphenyl)-2,2' :6', 2''-terpyridine))_2][PF_6]_2$, $[Os(tpybenzCOOH)_2][PF_6]_2$

To a suspension of tpybenzCOOH (217mg, 0.615mmol) in deaerated hot ethylene glycol (20ml) was added $OsCl_3.3H_2O$ (91.2mg, 0.308mmol), and the reaction was allowed to reflux for 4d under N_2. Reaction progress was monitored using TLC (MeCN /H_2O/20% KNO_3; 80:20:1). Following cooling at room temperature, a saturated aqueous solution of NH_4PF_6 was added. The dark precipitate was filtered and washed with water and dried with diethyl ether. Column chromatography on silica using the aforementioned mobile phase gave a dark maroon solid (100mg, 27.3%)

^{1}H NMR (400MHz, DMSO-d_6): δ (ppm) 9.55 (4H, s), 9.10 (4H, d, J=7.2Hz), 8.60 (4H, J=6.8Hz), 8.31-8.36 (m, 4H), 7.96 (q, 4H, 7.6Hz), 7.46 (4H, d, J= 5.6Hz), 7.23 (q, 4H, 6Hz). HR-MS(ESI-TOF) m/z: calculated for $C_{44}H_{30}N_6O_4Os$ $[M^{2+}]$: 449.0966; found: 449.0529.

Preparation of Os(II) bis- peptide conjugates:

$[Os(tpybenz-Ahx-MPP)_2].2(Cl^-)$, Os^{II} MPP

$[Os(tpybenzCOOH)_2][PF_6]_2$ (4.46mg, 1equiv) was weighed out directly into a glass vial followed by the addition of PyBOP (15.6mg, 8equiv), DIPEA(40equiv) and qualitative transfer of MPP peptide (20mg, 4equiv) with DMF (700µl). The mixture was allowed to stir at room temperature in dark overnight.

The reaction mixture was added dropwise to stirring saturated NH_4PF_6 (aq) to obtain dark brown solids that were collected via vacuum filtration, washed with water and dried with diethyl ether. The solids were dissolved in minimal acetone and added to a tetrabutylammonium chloride/acetone solution in order to obtain the chloride salt of the conjugate. The solids were washed with plentiful acetone and dried with diethyl ether yielding Os^{II} MPP. Purity

of the conjugate relative to the parent complex was confirmed by analytical Reverse Phase-HPLC and High-Resolution LCMS.

^{1}H NMR (600MHz, MeOH-d_4): δ (ppm) 9.35 (s, 4H), 8.89 (d, 4H), 8.40 (s, 8H), 8.21-7.88 (m, 7H), 7.46 (m, 4H), 7.22 (m, 40H), 4.58-3.31 (m, 31H), 3.23-2.81 (m, 20H), 2.34-2.12 (s, 47H), 2.08-1.06 (m, 64H). HR-MS (+)-MALDI *m/z*: calculated for $C_{180}H_{230}N_{42}O_{22}Os$ indicative of [M-MPP^{5+}+Cl$^-$]: 739.7249, found: 739.4184.

Photophysical Methods

Stock solutions (1mM) of the Os (II) parent and conjugate compound were prepared in MeCN or DMSO respectively and diluted in PBS for the preparation of working solutions. For oxygen measurements, the working solutions were purged with Nitrogen for 15minutes for de-aerated conditions and were allowed to re-aerate over time. The [O_2]/ µmol L^{-1} was measured using a PreSense Oxygen probe. The emission spectra and lifetimes were recorded at O_2 saturated and de-aerated conditions. Photostability studies were performed using a fan-cooled 150 W Orwell Xenon-Arc lamp on solutions of Os-complex in PBS pH 7.4. All photophysical studies were carried out at room temperature.

Cyclic Voltammetry

A CH 660 electrochemical analyzer was used to record cyclic voltammetry (CV). Stock solution of the complex was prepared as 1mM/ 0.1 M $TBAPF_6$ (supporting electrolyte) in anhydrous acetonitrile. The electrochemical cell used a Ag/AgCl reference electrode, Pt- wire counter and glassy carbon working electrode. CV measurements were performed in triplicate using positive scan polarity and 5mV s^{-1} scan rate.

Cell culture

Minimum Essential Medium Eagle (MEME); supplemented with 10% foetal bovine serum and 1% penicillin/ streptomycin and L-Glutamine (2 mM) was used as HeLa cell culture media. Dulbecco's Modified Eagle Medium (DMEM); supplemented with 10% foetal bovine serum, 1% penicillin/ streptomycin and L-Glutamine (2mM) was used to culture the MCF 7 cell line. Cells were grown at 37°C with 5% CO_2 and harvested or split at 90% confluency (using 1X Trypsin for 5 min at 37°C).

Cytotoxicity

HeLa cells were seeded in a 96- well plate in 100µl media at 10^4 cells/ well for 24h at 37°C under 5% CO_2. Os^{II} MPP was added in triplicate at the following final concentrations: 150, 100, 50, 25, 10, 1 and 0.1 µM. Control samples were prepared with 1% and 0.5% DMSO. Following 24 h incubation of the complex, 10 µl of Resazurin reagent was added to each well and incubated for 7h in the dark at 37°C. The Alamar Blue assay was used to estimate viable cells based on the absorbance measured at 570nm with a background measured at 600nm using a Tecan 96-well plate reader. The cytotoxicity study was carried out in triplicate.

Confocal luminescent Imaging

HeLa cells were seeded at 1.5 x 10^5 cells in 35mm glass-bottom culture dishes (Ibidi, Germany) of 2mL total volume. Cells were allowed to grow for 48h at 37°C at 5% CO_2. The growth medium was removed, and specific concentration of the complex was added and allowed to incubate for 4h at 37°C at 5% CO_2 in the dark. The dye/media solution was removed, and cells were washed with supplemented PBS (1.1mM $MgCl_2$ and 0.9mM $CaCl_2$). For live cell imaging, cells were directly imaged using a Leica TSP DMi8 confocal microscope (100X oil immersion objective lens) with a heated stage at 37°C. Os^{II} MPP was excited using a 490 nm white light laser and the emission range was set to 650 and 800 nm. DRAQ7, a nuclear staining dye was added (3µM) to distinguish intact live cells from permeabilized/ dead cells. The 633 nm laser was used to excite DRAQ 7 and emission was collected between 635-800nm. MitoTracker Deep Red, a cell permeable probe used to selectively stain mitochondria, was excited at 644nm and emission was collected between 655-720 nm.

Mitochondrial Depolarization Assay

The MitoPT TMRE Assays (ImmunoChemistry Technologies) were carried out on HeLa and MCF 7 cells. Cell populations were cultivated at 5 x 10^5 cells/ mL and MitoPT spiked suspensions of >3 x 10^6 cells/mL in 100µl/ well aliquots were prepared. The following control populations were prepared for each cell line: (A) negative control 1 (non-treated) (B) negative control 2 DMSO (100µM/ 1h), (C) positive control CCCP (20µM/ 1 h). Experimental populations were exposed to Os^{II} MPP at concentrations and incubation periods indicated by confocal imaging. Samples were subsequently incubated with MitoPT TMRE dye for 30 minutes at 37°C and washed. Aliquots were analyzed in triplicate (3 x 100 µl) in a black bottomed 96-well plate using Tecan Plate fluorescence plate reader set at 540nm excitation and 574 nm emission. The amount of orange fluorescence from TMRE was measured as an indication of metabolically stressed cells and mitochondrial depolarization. Data were quantified and expressed as the

View Article Online
DOI: 10.1039/C9DT02967B

percentage cell viability decline based on loss of mitochondrial membrane potential relative to the control cell populations.

Caspase Activity

Polycaspase FAM-FLICA assays (ImmunoChemistry Technologies) were carried out on HeLa and MCF 7 cells. Cells were cultivated at 3 x 10^5 cells/well. The following control populations were prepared for each cell line: negative control 1 (non-treated) (B) negative control 2 DMSO (100µM/ 1 h) (C) positive control (staurosporine 1µM/ 3 h). Experimental populations were exposed to Os^{II} MPP at specific concentration and incubation times based on confocal imaging findings. Samples were subsequently spiked with 30X FAM-FLICA for 45 minutes at 37°C. The loss of non-adherent cells during washing was accounted for by spinning down the overlay media and recombining the washed cell pellets with the overlay buffer prior to analysis. Samples were analyzed in triplicate (3 x 100 µl) in a black bottomed 96-well plate using Tecan Plate fluorescence plate reader set at 488 nm excitation and 520 nm emission. Poly caspase activity was monitored by the increase of relative fluorescence units (RFU) of the green fluorescent signal in the apoptotic cell populations. Data were quantified and expressed as the percentage of apoptotic cells based on the positive control cell populations.

Results and discussion

Synthesis

We exploited a tridentate, terpyridine-based ligand to facilitate the synthesis of an achiral Os (II) parent complex which, with carboxyl termini, allow for the bis-conjugation of the complex without the formation of multiple isomers. The synthetic route, and the molecular structures of the ligands and complex are summarized in Scheme 1. TpybenzCOOH was prepared according a modification of a previously reported syntheses.[43,44] And, $[Os(tpybenzCOOH)_2]^{2+}$ was synthesized by modifying a procedure reported for the synthesis of another tridentate Os(II)-complex.[45] Peptide conjugation to $[Os(tpybenzCOOH)_2]^{2+}$ was accomplished by amide coupling aided by PyBOP/DIPEA to yield bisconjugated $[Os(tpybenz\text{-}Ahx\text{-}MPP)_2]^{8+}$.[35,46] The MPP sequence used is a 8-amino acid mitochondrial localization sequence FrFKFrFK (r= D-arginine) originally reported by Kelley et al[47,48] which we have found to be highly effective in driving metal complexes to the mammalian mitochondria.[49] The lysine (K) and arginine residues provide positive charge and phenylalanine (F) imparts lipophilicity. ^1H NMR spectroscopy, Mass

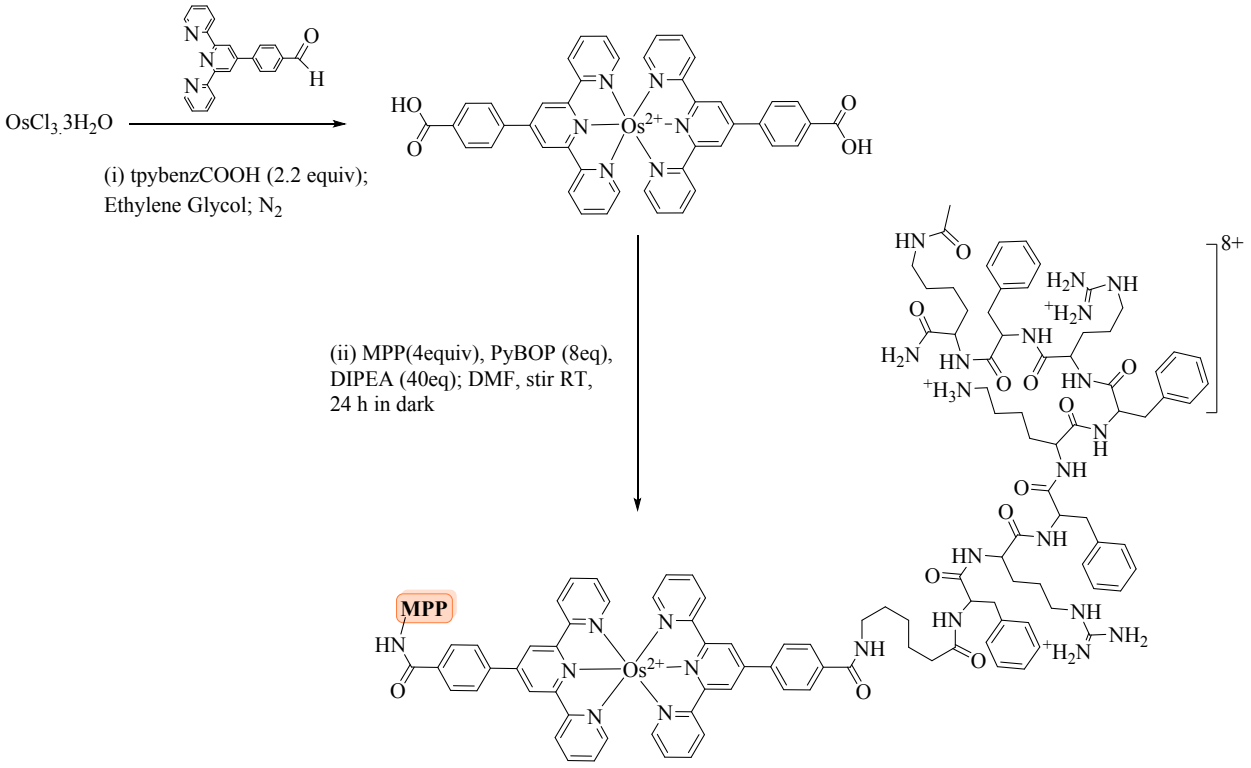

Scheme 1: Synthetic scheme for the preparation of Os^{II} MPP conjugate complex

spectrometry and HPLC analysis confirmed the structure and purity of the parent complex and peptide conjugate. RP-HPLC in absence of gradient confirmed formation of the complex and conjugate with well resolved peaks with retention time of 2.33 min for the parent complex and 3.13 min for the conjugate with no evidence for free peptide or unreacted parent in the latter case (ESI). With gradient elution, using 0.1% v/v TFA in MeCN and deionised water (Table 1) the retention time of the peptide conjugate was extended to 8.30 min but showed band broadening with peak splitting tentatively attributed to ion-pairing but. The corresponding chromatograms and UV/vis spectra, collected using diode array detection, confirm the band only contains metal complex, with no evidence for free peptide or unreacted starting complex (shown in the ESI).

Photophysics and Electrochemistry

The absorbance and emission spectra of the peptide conjugate, Os^{II}MPP, is shown in Fig. 1, analogous optical/photophysical behaviour was observed in the parent complex $[Os(tpybenzCOOH)_2]^{2+}$ (ESI†). The $Os(d_\pi)$-tpybenzCOOH (π^*) metal to ligand charge transfer transitions are observed at λ_{max} 490 nm (^{1}MLCT) and 663 nm (^{3}MLCT). Excitation at 490 nm into the singlet transition of the parent complex results in a relatively intense emission centered at 750 nm, and in aerated acetonitrile the quantum yield was determined as 0.0115 ± 0.0012. Under aerated conditions, the parent complex exhibits a lifetime of **129.9 ± 0.2 ns** in aqueous PBS (pH 7.4) which is increased to **183.3 ± 0.3 ns** on deaeration at room temperature. The photophysical data for the parent are consistent with those reported for a related phenyl derivative $[Os(phtpy)_2]^{2+}$ albeit with red-shifted emission maxima and modification to lifetime attributed to the carboxylate substitution of the phenylterpyridine ligands here.[45] The peptide conjugate, Os^{II} MPP exhibits mono-

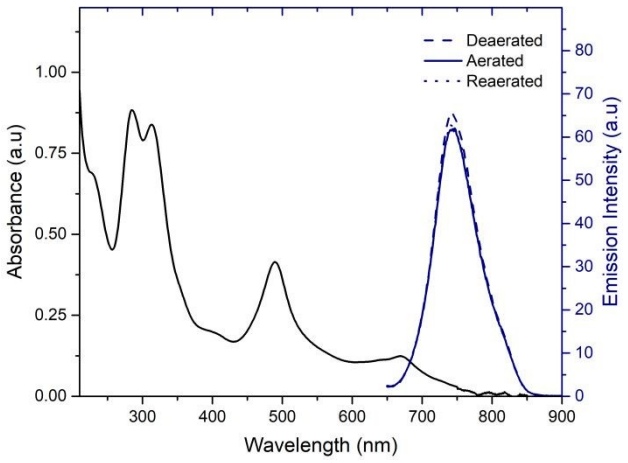

Figure 1: Absorbance and emission spectra of Os^{II}MPP. Spectra were recorded at 25μM (PBS Buffer pH 7.4) under aerated and deaerated conditions with excitation and emission slit widths of 10nm and emission excitation wavelength of 490 nm.

exponential emission decay but, surprisingly, is somewhat shorter-lived than the parent complex with a lifetime of 94.1 ± 0.4 ns in air saturated PBS that increases only to 110 ± 0.5 ns upon deaeration and a quantum yield of 0.0084 + 0.0005. The emission spectra were also compared under air saturated and upon deaerated conditions under nitrogen. As shown, corresponding to the lifetime data, the emission intensity of the conjugate does not respond significantly to change in $[O_2]$. Table 2 summarizes the photophysical properties of the parent and conjugate complex. This behaviour contrasts with our previous reports on ruthenium polypyridyl peptide conjugates, including complexes bound to the same MPP sequence.[49,35] There, the lifetime of emission invariably increased in the peptide conjugate compared to the parent. The origin of the decrease with the osmium complex is unclear, as the thermodynamics of electron transfer seem to preclude quenching so the effect may be due to steric strain exerted on the terpy ligand in the conjugate, that increases non-radiative decay. Nonetheless, the effect is relatively weak, and the osmium peptide conjugate remains sufficiently luminescent for imaging, without the complication of being a significant generator of singlet oxygen. As photostability is an important issue in bioimaging, this was evaluated for $[Os(tpybenzCOOH)_2]^{2+}$ in PBS buffer by monitoring its absorbance spectrum during visible irradiation. Following 3 hours continuous irradiation by a 150 mW arc lamp (using a λ>400 nm cut off filter) less than 5% photodegradation had occurred (ESI†). This renders the ^{3}MC state thermally inaccessible for Os(II) complexes in contrast to their Ru(II) analogues, particularly those of terpyridine complexes, that, as described tend to exhibit poor photophysical properties and photoinstability.

View Article Online
DOI: 10.1039/C9DT02967B

Table 1 Summary of photophysical properties of Os(II)- complexes in MeCN and PBS under aerated and deaerated conditions.

Compound	Solvent	λ_{abs} (ε)/ nm (x 10^4 M^{-1} cm^{-1})	λ_{em} /nm	τ /ns ± SD	
				Aerated	Deaerated
$[Os(tpybenzCOOH)_2]^{2+}$	CH_3CN	**404**(0.83), **490** (2.54), **642**(0.51), **670** (0.61)	750	120 ± 0.2	194.6.1 ± 0.7
	PBS	**418** (1.90), 5**05**(2.67), **648**(1.32), **679**(1.54)	745	129.9 ± 0.2	183.3 ± 0.3
$[Os(tpybenz\text{-}Ahx\text{-}MPP)_2]^{8+}$	PBS	**418**(0.26), **505**(0.47), **648**(0.14), **679**(0.15)	746	94.1 ± 0.4	110 ± 0.5

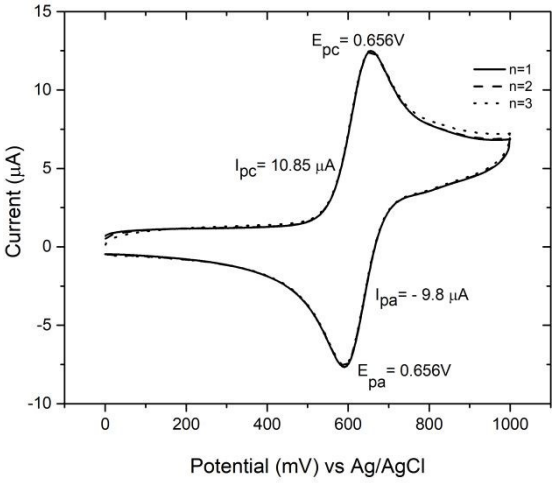

Electrochemistry of the parent complex is shown in Fig. 2. The complex shows well-behaved electrochemistry with a reversible anodic process attributed to the Os^{II}/Os^{III} oxidation at $E_{1/2}$ 656 mV versus Ag/AgCl in CH_3CN/ nBu_4NPF_6. The observed photostability, large stokes shift and modest O_2 quenching, marked these compounds as potentially attractive for cellular imaging applications. In particular, since in comparison to another reported Os(II) mono- conjugate, applied to cell imaging, the quantum yield of this conjugate is significantly higher (*φ = 0.0025 ± 0.0008*).[46]

Figure 2: Cyclic Voltammogram (n=3) of 1mM $[Os(tpybenzCOOH)_2]^{2+}$. Sample in deaerated CH_3CN containing 0.1M nBu_4NPF_6. Scan rate 50mV s^{-1}.

Cell Uptake studies

The uptake of $[Os(tpybenzCOOH)_2]^{2+}$ and Os^{II} MPP were evaluated in two cell lines: HeLa and MCF, as a function of conjugate concentration between the range 5μM and 50μM. While the parent complex does not permeate the cell membrane across this concentration range (see ESI†), the peptide conjugate is taken up by the cells at 30μM within 1 to 2 hours incubation in the absence of light (Fig. 3). Within 2h incubation, highly localized emission was observed from small structures thought to be the mitochondria. The distribution of the dye remained unchanged over the next 1 to 2 hours but as shown in Fig. 3, by 4 hours, morphological changes to the cells were evident including plasma membrane blebbing and retraction of pseudopods, indicating cell death by apoptosis. During this process, the probe started to leach from the mitochondria and at cell death (confirmed by DRAQ7 assay), the probe was evident in the cytoplasm attributed to loss of integrity of the mitochondrial membrane. At higher concentrations (Fig. 4, 50μM) the uptake dynamics and distribution were significantly different. Uptake was far more rapid and complete in under 1 hour. Confocal Z- scan shows (Fig. 4A) that at higher concentrations Os^{II} MPP was no longer confined to the mitochondria but present throughout the cytoplasm where it had penetrated the nuclear envelope and localised in the nucleoli. DRAQ 7 was applied to cells pre-incubated with the osmium conjugate to assess cell viability. DRAQ 7 is a far-red fluorescent probe which only stains the nuclei of damaged or dead cells. As shown in Fig. 4B, nuclei staining in blue shows that DRAQ 7 has entered the nuclei of essentially all cells indicating extensive cell death. Uptake of the dye and cell blebbing was observed when cells were incubated with complex above 40μM. This was surprising given the stability of the probe and lack of oxygen dependent emission. As they may offer therapeutic prospects we carried out more detailed investigation into the origin of the cytotoxicity.

View Article Online
DOI: 10.1039/C9DT02967B

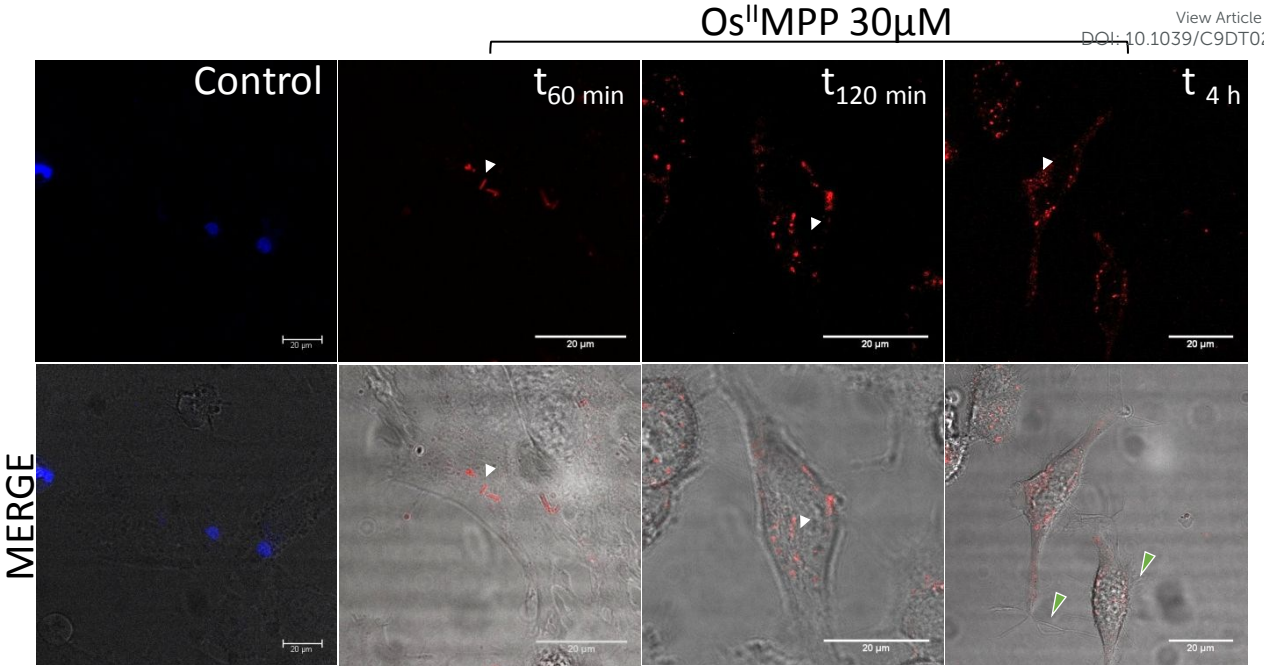

Figure 3: Confocal luminescence images of Os^{II} MPP in live HeLa cells where the conjugate and overlay channel are shown. Cells were incubated in the absence of light with 30µM for: 60 min, 120 min and 4 hr. The bis-MPP complex was excited using 490 nm white light laser and the emission was collected between 590 and 800nm.

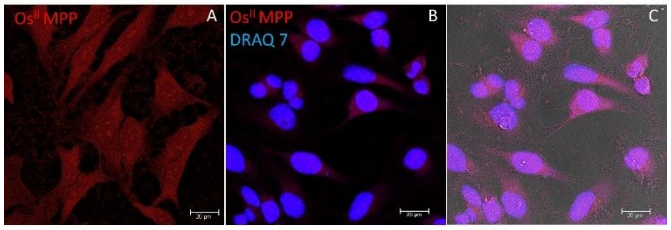

Figure 4: Confocal imaging: (A) Os^{II}MPP at increased concentration (50µM) in HeLa cells following 1hr incubation in the absence of light; z-scan reveals nucleoli staining (b) co- staining with DRAQ 7 and (c) overlay image

Os^{II} MPP : Co- localization with MitoTracker Deep Red in live HeLa cells

Co-localization with MitoTracker Deep Red confirmed the Os^{II} MPP probe localized at the mitochondria at concentrations below 30µM/ 2 h. Fig. 5 shows separate and super-imposed images of Os^{II} MPP and MitoTracker Deep Red and the corresponding line profile scanning in the x-y direction (B). Absence of nuclear staining by DRAQ 7 (ESI†) confirms viability of the cells. The line profile across the cell and the corresponding fluorescence intensity profile confirms co-localisation of the osmium conjugate and MitoTracker Deep Red in HeLa cells (Fig. 5B). In a previously reported $[Os(bpy)_2(pic\text{-}arg_8)]^{10+}$ conjugate, partial localization in both mitochondria and lysosomes in CHO cells was observed.[46] In addition, it was observed that the conjugate penetrated the nuclear envelope of SP2 myeloma and CHO cells via a photo or thermally- activated process. In contrast, we observed strong confinement of the dye below 30µM to the mitochondria and distribution does not change under irradiation. Distribution is found to change over extended intervals where coincident with DRAQ 7 permeation, the probe is found to leach into the cytoplasm and around the

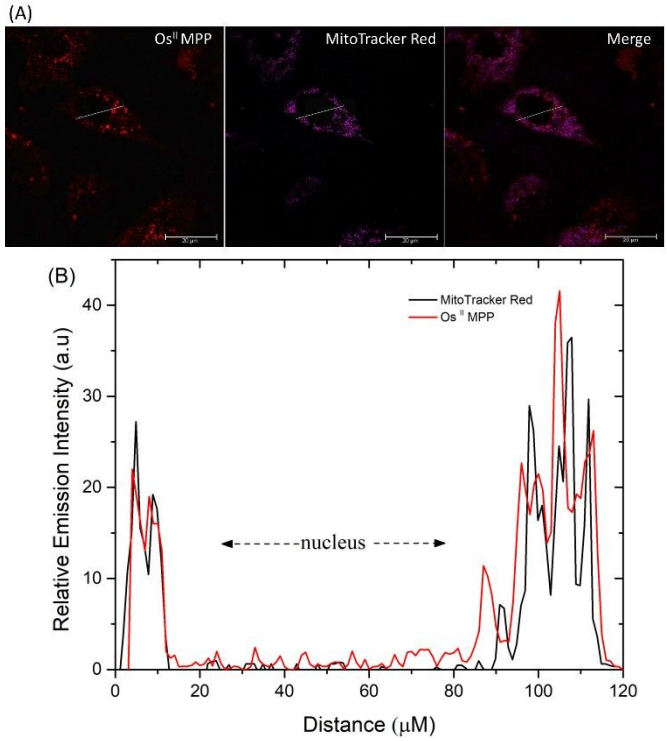

Figure 5: Co- localization of Os^{II} MPP with MitoTracker Deep Red where: (A) Confocal imaging of Os^{II} MPP (red), MitoTracker (purple) and merged image (B) Fluorescence intensity profiles obtained from the line profile across the cell (Image J). The cells were also co-incubated with DRAQ7 and absence of nuclear staining confirms cells are live.

nuclear envelope, potentially the endoplasmic reticulum (ER). Whereas this is the first , mitochondrial directed osmium luminophore to be reported, Ruthenium-MPP conjugates previously reported have shown mitochondrial confinement following 2 h incubation.[35,49]. The concentration dependent uptake observed here was not seen in comparable ruthenium complexes which exhibited only moderate toxicity in the dark following 24 h exposure over a range of concentrations. For example, HeLa cells were tolerant to the MPP-bridged dinuclear Ru (II) at 75µM over periods of 4-6 h of imaging and in the case of the Ru-dppz, cell death was induced only under intense photoirradiation.

Os^{II} MPP cytotoxic effects: photo-induced or intracellular triggered process?

Os^{II} MPP : Photo-toxicity studies in live HeLa cells

Given the phototoxicity of MPP-Ru complexes, phototoxicity was assessed in order to understand if the morphological changes observed during confocal imaging originated from photo-induced effects. In cells pre-incubated with 30µM Os^{II} MPP, single cells were selected and irradiated over time with increasing laser power (from 0.2µW to 0.9µW). As shown in Fig. 6, no DRAQ 7 was found to enter the nuclei of individual cells following continuous irradiation for 20 minutes at 490 nm. This confirmed that the is cytotoxicity is not light induced. This is not surprising given the remarkable photostability of the complex and weak oxygen dependence.

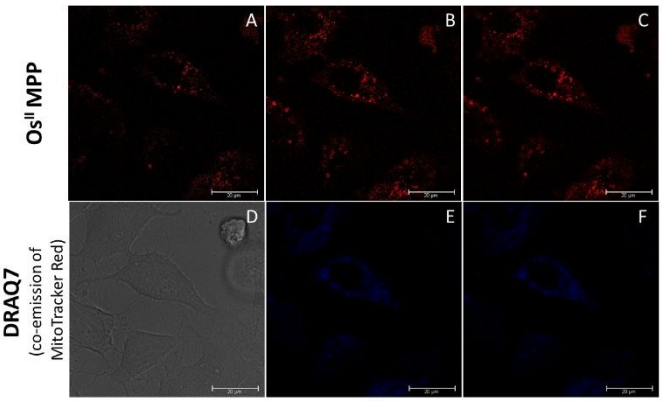

Figure 6: Phototoxicity of Os^{II} MPP (30µM) in HeLa cells using excitation with 490nm and scanning using increased laser power. (A, D) Normal imaging conditions (10% laser power) before scanning, (B, E) after 10 minutes scanning at 30% laser power and (C, F) additional 20 minutes scanning at 50% laser power; Observed in blue is the emission of MitoTracker Deep Red due to co-excitation of MitoTracker Deep Red at 633 nm.

Cytotoxicity

The viability of mammalian cells treated with Os^{II} MPP was assessed by incubating HeLa and separately, MCF 7 cells, with the conjugate in the absence of light overnight at 37°C. Cell death was investigated using the Alamar Blue viability assay. Reduction of resazurin dye to resorufin is used as a direct indicator of metabolically active cells. Both HeLa and MCF 7 cell lines presented poor tolerance to the Os^{II} MPP at concentrations above 40µM (see ESI†). This coincides with the confocal imaging studies where 40 - 100µM of dye induced cell death within 60 min incubation. HeLa cells were shown to be more tolerant to Os^{II} MPP at lower concentrations (5-30µM), with an IC_{50} value of 30.61µM, in comparison to MCF 7 cells where viability of 35% was observed upon incubation with the probe. These findings confirm that cell death is triggered by Os^{II} MPP in a dose dependent manner that seems to follow the trend observed in the concentration dependent uptake. We evaluated the mitocondrial potential and caspase activity to understand if the cytotoxicity observed originates at the mitochondria and if this switches at higher concentration.

Mitochondrial depolarization assay (Mito PT TMRE) and Caspase Activity

In healthy cells, an electrochemical potential is generated across the mitochondrial membrane due to the redox activity of the mitochondrial electron transport chain.[50] During apoptosis, the loss of mitochondrial membrane potential (MMP) coincides with the opening of the mitochondrial permeability transition pores, leading to the release of cytochrome c into the cytosol, which in turn triggers other downstream events in the apoptotic cascade. The mitochondrial membrane potential of cells can be assessed using the MitoPT TMRE assay. This assay uses a lipophilic and highly soluble rhodamine-based dye, TMRE, that penetrates live cells and accumulates within healthy mitochondria exhibiting fluorescence upon excitation. With loss of mitochondrial $\Delta\Psi_m$, TMRE is released into the cytosol resulting in a reduced fluorescence signal. Therefore, TMRE dye is used to detect apoptotic cell populations and to assess the mitochondrial membrane potential under varying conditions.[51,52] We performed MitoPT TMRE assays on HeLa and MCF 7 cells. Cell populations were prepared and then exposed to the assay conditions (ESI†). Two negative controls were prepared: a non-exposed cell population and a cell population exposed to DMSO. A positive control was also prepared by exposing the cells to CCCP, an agent known to cause mitochondrial depolarization. Experimental cell populations were exposed to Os^{II} MPP at a low concentration, 30µM/ 2 h at 37°C, where confocal imaging confirmed mitochondrial targeting and at at a higher concentration, 100µM/ 1 h at 37°C, where imaging and cytotoxicity studies

showed wide probe distribution and poor cell viability. Following exposure to the experimental conditions, cell populations were spiked with MitoPT dye and incubated for 30 minutes at 37°C. Fig. 7 summarizes the results of the assay. As expected, the percentage of viable cells decreased significantly upon exposure to the CCCP agent, validating the assay. Decreased cell viability was also observed for the population of cells exposed to Os^{II} MPP 30µM/ 2 h indicating that cells were undergoing metabolic or apoptotic stress that can be attributed to collapse of the mitochondrial potential. Confocal imaging under these conditions had shown mitochondrial targeting and initiation of blebbing but that cells were still viable according to DRAQ 7 co-staining. Over extended exposure collapse of the mitochondrial membrane potential gradually leads to irreversible mitochondrial damage triggering cell death and thus leakage of the Os^{II} MPP probe from the cells. Interestingly, consistent with concentration dependent localization observed from confocal imaging, although some mitochondrial depolarization was also evident for cells exposed to Os^{II} MPP at 100µM/ 1 h, the number of apoptotic cells due to collapsed $\Delta\Psi_m$, was significantly lower for Os^{II} MPP 100µM/ 1 h than for 30µM/ 2 h. Therefore, we conclude that the altered localization of the probe at increased concentrations elicits the cytotoxic effect from a mechanism different to that observed at lower concentrations.

Mitochondrial apoptotic effectors released upon mitochondrial depolarization can be triggered outside the mitochondria by initiation of a cascade of caspase activation leading to apoptosis.[5] Given that the cytotoxicity is greater at higher Os^{II} MPP concentrations but that mitochondrial depolarization, coincident with localization of Os^{II} MPP to the mitochondria is more prevalent at lower concentrations we examined the caspase activity induction ability of Os^{II} MPP in cells using the FLICA assay to evaluate caspase activity as a function of probe concentration.

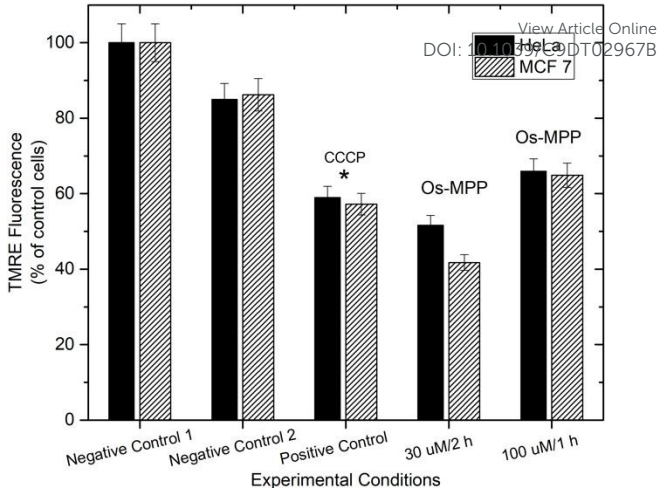

Figure 7: Relative Fluorescence Units obtained by MitoPT Assay (n=3) expressed as a percentage of the negative control. HeLa and MCF 7 cells were exposed to DMSO (100µM/ 1 h) (negative control 2) and CCCP depolarizing agent (positive control). Experimental populations were exposed to Os^{II} MPP under the conditions previously described. All samples were incubated with MitoPT TMRE for 30 minutes at 37°C and washed. Aliquots were added in a black 96-well plate in triplicate and analysed by Tecan fluorescence plate reader set at 540 nm excitation and 574 nm emission. Healthy cells exhibited a high level of orange fluorescence whereas metabolically stressed cells (positive control and Os^{II} MPP treated) exhibited a reduced fluorescence signal indicating MMP depolarization. Illustrated is the percentage cell viability decline based on loss of mitochondrial membrane potential relative to the non-exposed (negative control) cell populations.

Caspase Activation assay

In the caspase assay applied here, caspase activity is monitored via the green fluorescence signal from the FLICA probe, a carboxyfluoroscein fluorophore with a fluoromethyl ketone unit that bonds covalently to an active caspase enzyme. Unbound FLICA diffuses out of the cell and is removed during the wash steps prior to analysis. Experimental populations were prepared where staurosporine, known for caspase-3 activation,[53] was used to induce caspase activity (positive control) in both cell lines. Identical conditions of OsIIMPP concentration and incubation times were used here as for the MitoPT Assay. As shown in Fig. 8, Os^{II} MPP at 30uM/ 2 h stimulated caspase activity in the MCF 7 cell line which corresponds with the confocal imaging which showed that imaging of mitochondrial targeting was possible for HeLa cells without cell damage whereas MCF 7 cells showed higher sensitivity to the Os^{II} MPP complex. In addition, a higher apoptotic percentage was observed for the 100µM/ 1 h probe incubation. Therefore, according to the MitoPT and FLICA assays findings, at Os^{II} MPP concentrations exceeding 40 µMl is a moderate release of apoptotic factors owing to collapse of $\Delta\Psi_m$ but localization of the probe in other regions of the cell triggers activation of caspase enzymes leading to

apoptosis. At lower concentrations (30μM/ 2 h), when the complex localizes at the mitochondria, this stimulates the release of mitochondrial apoptotic effectors, owing to depolarization of MMP, and caspase activity is observed to a lesser extent.

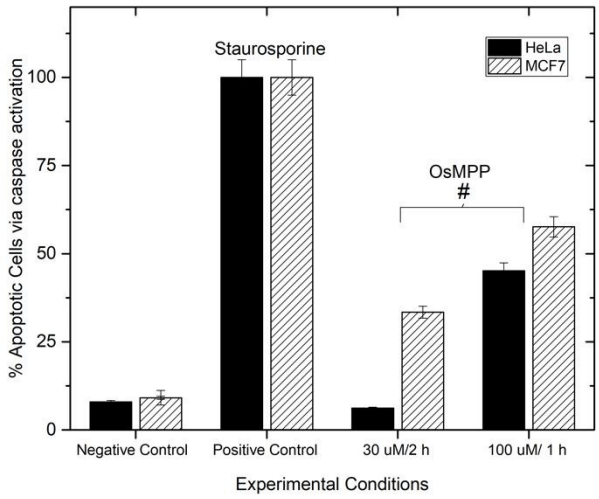

Figure 8: The percentage of cells showing caspase activity indicative of apoptosis obtained by FLICA Assay (n=3). Both cell lines were exposed to DMSO as a second negative control (S.I) and Staurosporine as the positive control. Experimental populations were exposed to Os^{II} MPP at 30μM/ 2 h and 100μM/ 1 h. All samples were incubated with 30X FLICA reagent for 45 minutes at 37°C followed by two washing steps and re-suspension of spun down pellets. Aliquots were analyzed in a black 96-well plate by Tecan fluorescence plate reader set at 488 nm excitation and 520 nm emission. Healthy cells exhibited minimal green fluorescence whereas apoptotic cells due to caspase activity exhibited a green fluorescence signal.

It is plausible that this causes initiation of the mitochondrial (intrinsic) apoptotic pathway leading to cell death but allows for confocal imaging of the mitochondrial structures between 2 to 3 h incubation period. In contrast, increased concentrations of the conjugate lead to rapid uptake and wide distribution of the Os^{II} MPP probe, in both HeLa and MCF 7 cells, which leads to mitonuclear communication and in turn, release of mitochondrial apoptotic effectors and caspase cascade activation.[54,55] Related Ru^{II} polypyridyl complexes have been rerouted from nuclear DNA to mitochondrial targeting by controlling the delivery and uptake mechanism of the probes[54] thus highlighting the potential of these complexes in achieving change in activity based on cellular delivery and localisation.

Conclusions

A novel achiral Os (II) complex $[Os(tpybenzCOOH)_2]^{2+}$ was synthesized and characterised. Bisconjugation of a mitochondrial penetrating peptide (MPP) to both conjugatable sites of the parent complex was achieved by amide coupling reaction. Both parent and conjugate exhibited relatively intense NIR-emission that coincides well with the biological window. Excellent photostability and good quantum yield rendered the probe attractive for cellular imaging application. However, rather unusually, the conjugate showed modest reduction of its emission lifetime and quantum yield compared to the parent.

View Article Online
DOI: 10.1039/C9DT02967B

Cell uptake studies were explored in live HeLa and MCF 7 cells. While the parent complex was cell impermeable, confocal imaging and co-localisation studies with MitoTracker Deep Red showed that the bis-MPP Os (II) system is membrane permeable and targets the mitochondria at concentrations below 50μM. With increased concentration, Os^{II} MPP showed rapid uptake and wider distribution including penetration of the nuclear envelope and localisation in the nucleoli structures. Extensive cell death was confirmed with DRAQ 7 staining. Photocytotoxicity studies did not show any evidence for photo-induced cytotoxic effects. Loss in TMRE signal indicating mitochondrial depolarization was observed at Os^{II} MPP 30μM/ 2h where the probe localises solely at the mitochondria, caspase activity at these conditions was moderate with increased activity observed in MCF 7 over HeLa cells. At higher concentrations (100μM/ 1 h), the MitoPT and FLICA assays showed increased caspase activity and lower degree of mitochondrial depolarization indicating a switch in cell death mechanism with delocalisation of the probe.

Conflicts of interest

There are no conflicts to declare.

Abbreviations

AIF	Apoptosis-inducing factor
CCCP	Carbonyl cyanide m-chlorophenyl hydrazone
DMSO	Dimethysulfoxide
DNA	Deoxyribonucleic Acid
F	Phenylalanine
IRF	Instrument Response Function
K	Lysine
MLCT	Metal-ligand charge transfer
MMP	Mitochondrial membrane potential

MPP	Mitochondria targeting peptide FrFKFrFK
PBS	Phosphate buffer saline
PyBOP	benzotriazol-1-yl-oxytripyrrolidinophosphonium hexafluorophosphate
r	Arginine
TMRE	Trimethylrhodamine, ethyl ester
tpybenzCOOH	4'- (4-Carboxyphenyl)-2,2' :6', 2''-terpyridine

Acknowledgements

KSG and TEK gratefully acknowledge the Irish Research Council Scholarship: IRC Government of Ireland Postgraduate Scholarship GOIPG/2016/702. This material is based upon work supported by Science Foundation Ireland under Grant No. [14/IA/2488] and [18/TIDA/5862]. The Programme for Research in Third Level Institutions (PRTLI) Cycle 4 and 5 is acknowledged for instrumentation under the NBIPI and NRF at Dublin City University. The PRTLI is co-funded through the European Regional Development Fund (ERDF), part of the European Union Structural Funds Programme 2007–2015. Professor Richard O'Kennedy, School of Biotechnology, DCU, is gratefully acknowledged for access to cell culture facilities.

Notes and references

‡ Footnotes relating to the main text should appear here. These might include comments relevant to but not central to the matter under discussion, limited experimental and spectral data, and crystallographic data.

1 M. R. Duchen and G. Szabadkai, *Essays In Biochemistry*, 2010, **47**, 115–137.
2 D. C. Wallace, *Nature Reviews Cancer*, 2012, **12**, 685–698.
3 A. Martin, A. Byrne, C. S. Burke, R. J. Forster and T. E. Keyes, *Journal of the American Chemical Society*, 2014, **136**, 15300–15309.
4 C. Sanchez-Cano, I. Romero-Canelón, Y. Yang, I. J. Hands-Portman, S. Bohic, P. Cloetens and P. J. Sadler, *Chemistry - A European Journal*, 2017, **23**, 2512–2516.
5 S. Wen, D. Zhu and P. Huang, *Future Medicinal Chemistry*, 2013, **5**, 53–67.
6 A. Levina, A. Mitra and P. A. Lay, *Metallomics*, 2009, **1**, 458.
7 A. Bonetti, R. Leone, F. M. Muggia and S. B. Howell, Eds., *Platinum and Other Heavy Metal Compounds in Cancer Chemotherapy*, Humana Press, Totowa, NJ, 2009.
8 S. M. Meier-Menches, C. Gerner, W. Berger, C. G. Hartinger and B. K. Keppler, *Chemical Society Reviews*, 2018, **47**, 909–928.
9 E. Alessio and L. Messori, in *Metallo-Drugs: Development and Action of Anticancer Agents*, eds. A. Sigel, H. Sigel, E. Freisinger and R. K. O. Sigel, De Gruyter, Berlin, Boston, 2018, pp. 141–170.
10 P.-S. Kuhn, V. Pichler, A. Roller, M. Hejl, M. A. Jakupec, W. Kandioller and B. K. Keppler, *Dalton Transactions*, 2015, **44**, 659–668.
11 R. Trondl, P. Heffeter, C. R. Kowol, M. A. Jakupec, W. Berger and B. K. Keppler, *Chem. Sci.*, 2014, **5**, 2925–2932.
12 S. Leijen, S. A. Burgers, P. Baas, D. Pluim, M. Tibben, E. van Werkhoven, E. Alessio, G. Sava, J. H. Beijnen and J. H. M. Schellens, *Investigational New Drugs*, 2015, **33**, 201–214.
13 D. Pluim, R. C. A. M. van Waardenburg, J. H. Beijnen and J. H. M. Schellens, *Cancer Chemotherapy and Pharmacology*, 2004, **54**, 71–78.
14 E. Meggers, *Chemical Communications*, 2009, 1001.
15 J. Maksimoska, D. S. Williams, G. E. Atilla-Gokcumen, K. S. M. Smalley, P. J. Carroll, R. D. Webster, P. Filippakopoulos, S. Knapp, M. Herlyn and E. Meggers, *Chemistry - A European Journal*, 2008, **14**, 4816–4822.
16 K. Suntharalingam, W. Lin, T. C. Johnstone, P. M. Bruno, Y.-R. Zheng, M. T. Hemann and S. J. Lippard, *Journal of the American Chemical Society*, 2014, **136**, 14413–14416.
17 G. Berger, K. Grauwet, H. Zhang, A. M. Hussey, M. O. Nowicki, D. I. Wang, E. A. Chiocca, S. E. Lawler and S. J. Lippard, *Cancer Letters*, 2018, **416**, 138–148.
18 K. Suntharalingam, T. C. Johnstone, P. M. Bruno, W. Lin, M. T. Hemann and S. J. Lippard, *Journal of the American Chemical Society*, 2013, **135**, 14060–14063.
19 C. Sanchez-Cano, I. Romero-Canelón, Y. Yang, I. J. Hands-Portman, S. Bohic, P. Cloetens and P. J. Sadler, *Chemistry - A European Journal*, 2017, **23**, 2512–2516.
20 C. G. Hartinger, N. Metzler-Nolte and P. J. Dyson, *Organometallics*, 2012, **31**, 5677–5685.
21 C. A. Riedl, L. S. Flocke, M. Hejl, A. Roller, M. H. M. Klose, M. A. Jakupec, W. Kandioller and B. K. Keppler, *Inorganic Chemistry*, 2017, **56**, 528–541.
22 B. Boff, C. Gaiddon and M. Pfeffer, *Inorganic Chemistry*, 2013, **52**, 2705–2715.
23 S. Lazic, P. Kaspler, G. Shi, S. Monro, T. Sainuddin, S. Forward, K. Kasimova, R. Hennigar, A. Mandel, S. McFarland and L. Lilge, *Photochemistry and Photobiology*, 2017, **93**, 1248–1258.
24 S. A. E. Omar, P. A. Scattergood, L. K. McKenzie, C. Jones, N. J. Patmore, A. J. H. M. Meijer, J. A. Weinstein, C. R. Rice, H. E. Bryant and P. I. P. Elliott, *Inorganic Chemistry*, 2018, **57**, 13201–13212.
25 Y. Sun, L. E. Joyce, N. M. Dickson and C. Turro, *Chemical Communications*, 2010, **46**, 6759.
26 A. Byrne, C. Dolan, R. D. Moriarty, A. Martin, U. Neugebauer, R. J. Forster, A. Davies, Y. Volkov and T. E. Keyes, *Dalton Transactions*, 2015, **44**, 14323–14332.
27 P. Zhang and H. Huang, *Dalton Transactions*, 2018, **47**, 14841–14854.
28 E. C. Glazer, *Photochemistry and Photobiology*, 2017, **93**, 1326–1328.
29 L. Blackmore, R. Moriarty, C. Dolan, K. Adamson, R. J. Forster, M. Devocelle and T. E. Keyes, *Chemical Communications*, 2013, **49**, 2658.

30 A. Byrne, C. S. Burke and T. E. Keyes, *Chemical Science*, 2016, **7**, 6551–6562.
31 U. Neugebauer, Y. Pellegrin, M. Devocelle, R. J. Forster, W. Signac, N. Moran and T. E. Keyes, *Chemical Communications*, 2008, 5307.
32 J. R. Shewring, A. J. Cankut, L. K. McKenzie, B. J. Crowston, S. W. Botchway, J. A. Weinstein, E. Edwards and M. D. Ward, *Inorganic Chemistry*, 2017, **56**, 15259–15270.
33 A. Byrne, C. Dolan, R. D. Moriarty, A. Martin, U. Neugebauer, R. J. Forster, A. Davies, Y. Volkov and T. E. Keyes, *Dalton Transactions*, 2015, **44**, 14323–14332.
34 A. Jana, B. J. Crowston, J. R. Shewring, L. K. McKenzie, H. E. Bryant, S. W. Botchway, A. D. Ward, A. J. Amoroso, E. Baggaley and M. D. Ward, *Inorganic Chemistry*, 2016, **55**, 5623–5633.
35 C. S. Burke, A. Byrne and T. E. Keyes, *Angewandte Chemie International Edition*, 2018, **57**, 12420–12424.
36 A. Byrne, C. Dolan, R. D. Moriarty, A. Martin, U. Neugebauer, R. J. Forster, A. Davies, Y. Volkov and T. E. Keyes, *Dalton Transactions*, 2015, **44**, 14323–14332.
37 X. Li, A. K. Gorle, T. D. Ainsworth, K. Heimann, C. E. Woodward, J. Grant Collins and F. Richard Keene, *Dalton Transactions*, 2015, **44**, 3594–3603.
38 J. P. Sauvage, J. P. Collin, J. C. Chambron, S. Guillerez, C. Coudret, V. Balzani, F. Barigelletti, L. De Cola and L. Flamigni, *Chemical Reviews*, 1994, **94**, 993–1019.
39 Y.-Q. Fang, N. J. Taylor, G. S. Hanan, F. Loiseau, R. Passalacqua, S. Campagna, H. Nierengarten and A. V. Dorsselaer, *Journal of the American Chemical Society*, 2002, **124**, 7912–7913.
40 Y.-Q. Fang, N. J. Taylor, F. Laverdière, G. S. Hanan, F. Loiseau, F. Nastasi, S. Campagna, H. Nierengarten, E. Leize-Wagner and A. Van Dorsselaer, *Inorganic Chemistry*, 2007, **46**, 2854–2863.
41 E. A. Medlycott and G. S. Hanan, *Chemical Society Reviews*, 2005, **34**, 133.
42 J. P. Collin, S. Guillerez, J. P. Sauvage, F. Barigelletti, L. De Cola, L. Flamigni and V. Balzani, *Inorganic Chemistry*, 1992, **31**, 4112–4117.
43 E. C. Constable, E. L. Dunphy, C. E. Housecroft, M. Neuburger, S. Schaffner, F. Schaper and S. R. Batten, *Dalton Transactions*, 2007, 4323.
44 A. Stublla and P. G. Potvin, *European Journal of Inorganic Chemistry*, 2010, **2010**, 3040–3050.
45 E. A. Alemán, C. D. Shreiner, C. S. Rajesh, T. Smith, S. A. Garrison and D. A. Modarelli, *Dalton Transactions*, 2009, 6562.
46 A. Byrne, C. Dolan, R. D. Moriarty, A. Martin, U. Neugebauer, R. J. Forster, A. Davies, Y. Volkov and T. E. Keyes, *Dalton Transactions*, 2015, **44**, 14323–14332.
47 K. L. Horton, K. M. Stewart, S. B. Fonseca, Q. Guo and S. O. Kelley, *Chemistry & Biology*, 2008, **15**, 375–382.
48 S. R. Jean, M. Ahmed, E. K. Lei, S. P. Wisnovsky and S. O. Kelley, *Accounts of Chemical Research*, 2016, **49**, 1893–1902.
49 A. Martin, A. Byrne, C. S. Burke, R. J. Forster and T. E. Keyes, *Journal of the American Chemical Society*, 2014, **136**, 15300–15309.
50 S. W. Perry, J. P. Norman, J. Barbieri, E. B. Brown and H. A. Gelbard, *BioTechniques*, 2011, **50**, 98–115.
51 A. Wong and G. A. Cortopassi, *Biochemical and Biophysical Research Communications*, 2002, **298**, 750–754.
52 D. L. Farkas, M. D. Wei, P. Febbroriello, J. H. Carson and L. M. Loew, *Biophysical Journal*, 1989, **56**, 1053–1069.
53 A. Stepczynska, K. Lauber, I. H. Engels, O. Janssen, D. Kabelitz, S. Wesselborg and K. Schulze-Osthoff, *Oncogene*, 2001, **20**, 1193–1202.
54 E. F. Fang, M. Scheibye-Knudsen, K. F. Chua, M. P. Mattson, D. L. Croteau and V. A. Bohr, *Nature Reviews Molecular Cell Biology*, 2016, **17**, 308–321.
55 P. M. Quirós, A. Mottis and J. Auwerx, *Nature Reviews Molecular Cell Biology*, 2016, **17**, 213–226.
56 X. Tian, M. R. Gill, I. Cantón, J. A. Thomas and G. Battaglia, *ChemBioChem*, 2011, **12**, 548–551.